Computation of Eddy Current Thin Plates by Using a Perturbation Method for Field – Circuit Coupled Problems by Coupling to Global Quantities

Vuong Dang Quoc[1], Hung Bui Duc[1,*], and Dinh Bui Minh[1]

ARTICLE INFO

ABSTRACT

The eddy current loss is one of important parts of total losses of transformers, which causes a reduced efficiency of the transformer. Recently, several methods (e.g., boundary finite element method, finite element method, subproblem method) to investigate and analyzed the influence and distribution of local quantities on the iron core, tank and shielding plate of distribution transformers. In this context, one-way coupling to global quantities considering as global current and voltage is proposed for computing the eddy current and joule power losses in shielding plates of transformers. This technique allows to couple local and global quantities in several steps. Each step is performed on an independent domain/mesh without dependence on to other domains/meshes.

Notation: Some symbols are given below:

H_h^0 (rot; Ω)	Curl-conform function space in Ω
$< \cdot, \cdot >$	Surface integral of the product of its vector field argument
$(\cdot, \cdot)$	Volume integral of the product of its vector field argument
H	Magnetic field (A/m)
B	Magnetic flux density (T)
E	Electric field (V/m)
D	Electric flux density (C/m^2)
$\mathbf{J}_s$	Electric current density (A/m^2)
J	Eddy current density (A/m^2)
$\mathbf{j}_f$	Surface source field
Ω	Bounded open set of E^3
Γ	Boundary of Ω ($\Gamma = \partial\Omega$)
μ	Magnetic permeability (H/m)
μ_r	Relative magnetic permeability
σ	Electric conductivity (S/m)
n	Unit normal exterior to Ω

1. INTRODUCTION

Many researchers have recently applied different methods, such as a traditional finite element method (FEM) and subproblem method (SPM) to evaluate eddy currents and joule power losses in the shielding plate of distribution transformers. The FEM was used in [1] to solve the above problems, but the direct application of this method for realistic structures is still very difficult due to the high aspect ratio of some parts of the transformer such as thin conducting regions, shielding plates and cover plates. In [2], authors also developed a sub-domain approach with the conform formulation to improve the accuracy of field calculations in thin shell (TS) models. Coupling is carried out in [2] without taking into account global variables such as current or voltage. In [3] and [4] a subproblem method was presented for treating errors on shielding models. In this study, the paper has used an *h*-conform formulation with a simply connected region to evaluate fields around the borders and corners of thin shells. In [5] and [6] a magnetic vector potential formulation was developed with subproblem technique for improvement of TS models between a double conductiong region, and between non-conducting and conducting regions. and for treating errors on shielding models. In [7]-[9] shielding structures were studied to minitage the influence of magnetic fields due to electric currents in power underground cables.

In this research, one-way coupling technique is extended with the *h*-conform finite element formulations for coupling to global quantities, such as global current and voltage. The developed approach is organized in several steps. The inital problem consists in a massive coil on which either current or voltage can be imposed. The next problem which can be (shielding/thin plates or cover plates is solved with a coarse mesh without considering the previous problem (a massive coild) anymore. The solutions obtained at this step are not

[1]*Department of Electrical Engineering, Hanoi University of Science and Technology.*
Corresponding author: Hung Bui Duc; E-mail: hung.buiduc@hust.edu.vn.

yet accurate, thus a final step with the actual mesh is required to correct TS soltuions. Next steps, it can be contrained by surface sources (SSs) or volume sources (VSs) already defined in [4]-[7]. In addition, the solutions of developed method have been also compared with the TS solution of subproblem methods [3]-[5].

2. MODELING OF MAGNETODYNAMIC PROBLEMS

2.1. General magnetodynamic problem

A model of electromagnetic problem is shown in Figure 2, where the BC ($\partial\Omega$) of studied domain (Ω) is as $\partial\Omega = \Gamma = \Gamma_h \cup \Gamma_e$. The terms I_i and V_i are respectively the global current and voltage expressed as quantities of an external circuit. The set of Maxwell's equations and the behavior laws is written in the frequency domain as [10]-[12]:

$$\text{rot } \mathbf{H} = \mathbf{J}_s, \tag{1}$$

$$\text{rot } \mathbf{E} = -j\omega \mathbf{B}, \tag{2}$$

$$\text{div } \mathbf{B} = 0, \tag{3}$$

$$\mathbf{B} = \mu\mathbf{H}, \quad \mathbf{J} = \sigma\mathbf{E}. \tag{4a-b}$$

In (1), the quantity $\mathbf{J}_s$ is considered as electrical current in the massive inductor.

The fields such as $\mathbf{B}$, $\mathbf{H}$, $\mathbf{E}$ are defined in Ω (with $\Omega = \Omega_c \cup \Omega_C^c$), where Ω_c is the conducting domain and Ω_C^c is the non-conducting one. The field $\mathbf{J}$ and $\mathbf{J}_s$ are defined in Ω_c. The boundary condition (BC) on Γ_e is

$$\mathbf{n} \times \mathbf{E}|_{\Gamma_e} = \mathbf{J}_f. \tag{5}$$

The fields ($\mathbf{B}$, $\mathbf{H}$, $\mathbf{E}$, $\mathbf{J}$) are determined to satisfy the function spaces (that contain the fields defined on Γ_h and Γ_e of studied domain Ω) in Tonti's diagram [10], that is, $\mathbf{J} \in \mathbf{H}(\text{div}; \Omega)$, $\mathbf{E} \in \mathbf{H}_e(\text{rot}; \Omega)$, $\mathbf{H} \in \mathbf{H}_h(\text{rot}; \Omega)$ and $\mathbf{B} \in \mathbf{H}_e(\text{div}; \Omega)$.
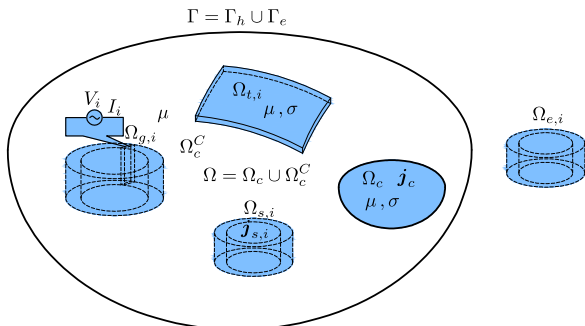
Fig. 1. General magnetodynamic model.

For global conditions, the current or voltage is considered as presented in Figure 2, where a source of the voltage V_i or current I_i between two electrodes of a domain $\Omega_{g,i}$ is defined through surface $\Gamma_{g,i}$, i. e [3].
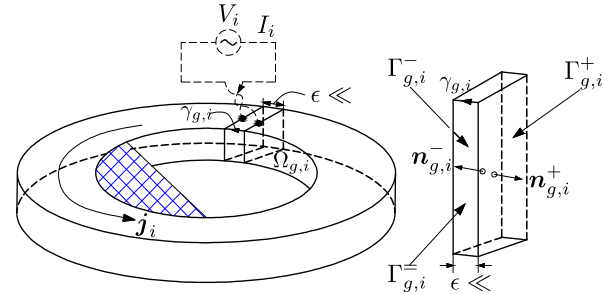
Fig.2. Coupling global current (I_i) and voltage (V_i) [10].

$$\oint_{\gamma_{g,i}} \mathbf{E} \cdot d\mathbf{l} = V_i \quad \text{and} \quad \oint_{\gamma_{g,i}} \mathbf{n} \cdot \mathbf{J} ds = I_i, \tag{6a-b}$$

where $\gamma_{g,i}$ is considered as the part of the boundary $\Gamma_{g,i}$ already presented in Figure 2.

2.2. Magnetic field intensity weak formulations

Based on the Maxwell's equation defined in (1), the field $\mathbf{H}$ can be split as [18, 19]:

$$\mathbf{H} = \mathbf{H}_r + \mathbf{H}_s - \text{grad } \varphi, \quad \text{for} \quad \text{rot } \mathbf{H}_s = \mathbf{J}_s, \tag{7}$$

where, $\mathbf{H}_r$ is the reaction field defined in Ω_c and $\mathbf{H}_s$ is the source field defined in Ω_C^c. The field φ is the magnetic scalar potential defined in Ω_C^c. It is a single value via the cuts [3]. The $\mathbf{H}$-conform weak formulation is written via the Faraday's law (1 b) and consititutive law (2a), i.e [19].

$$\partial_t(\mu\,\mathbf{H}, \mathbf{H}')_\Omega + (\mathbf{E}, \text{rot } \mathbf{H}')_\Omega + < \mathbf{n} \times \mathbf{E}, \mathbf{H}' >_{\Gamma_e - \Gamma_t} + < [\mathbf{n} \times \mathbf{E}]_{\Gamma_t}, \mathbf{H}' >_{\Gamma_t} = 0, \forall\, \mathbf{H}' \in \mathbf{H} \in H_h^0(\text{rot}; \Omega), \tag{8}$$

In Ω_c, the electric field $\mathbf{E}$ in (8) is defined by $\mathbf{E} = \sigma^{-1}\text{rot }\mathbf{H}$. Therefore, (8) can be rewitten as

$$\partial_t(\mu\,\mathbf{H}, \mathbf{H}')_\Omega + (\sigma^{-1}\text{rot } \mathbf{H}, \text{rot } \mathbf{H}')_{\Omega_c} + (\mathbf{E}, \text{rot } \mathbf{H}')_{\Omega_C^c}$$
$$+ < \mathbf{n} \times \mathbf{E}, \mathbf{H}' >_{\Gamma_e - \Gamma_t} + < [\mathbf{n} \times \mathbf{E}]_{\Gamma_t}, \mathbf{H}' >_{\Gamma_t} = 0,$$
$$\forall\, \mathbf{H}' \in \mathbf{H} \in H_h^0(\text{rot}; \Omega), \tag{9}$$

By combining (5) and (7), it should be noted that rot $\mathbf{H}_r$ = 0 in Ω_C^c. The test function $\mathbf{H}'$ in (7) belongs to subspace of $H_h^0(\text{rot}; \Omega)$. Thus, the term rot $\mathbf{H}_r' = 0$ in Ω_C^c, for $\mathbf{H}' = \mathbf{H}_s' + \mathbf{H}_r'$. In addition, the integral of $(\mathbf{E}, \text{rot } \mathbf{H}')_{\Omega_C^c}$ in (9) can be omitted. Therefore, (9) can be rewritten as

$$\partial_t(\mu\,\mathbf{H}_r, \mathbf{H}')_\Omega + (\sigma^{-1}\text{rot } \mathbf{H}_r, \text{rot } \mathbf{H}')_{\Omega_c} + (\mu\mathbf{H}_s, \mathbf{H}')_{\Omega_C^c} +$$
$$< [\mathbf{n} \times \mathbf{E}]_{\Gamma_t}, \mathbf{H}' >_{\Gamma_t} + < \mathbf{n} \times \mathbf{E}, \mathbf{H}' >_{\Gamma_e - \Gamma_t} = 0,$$
$$\forall\, \mathbf{H}' \in \mathbf{H} \in H_h^0(\text{rot}; \Omega), \tag{10}.$$

The trace discontinuity $< \mathbf{n} \times \mathbf{E}, \mathbf{H}' >_{\Gamma_e - \Gamma_t}$ is the BC for for coupling to the global quanity will be presented in Section 2.3, while the trace discontinuity $< [\mathbf{n} \times \mathbf{E}]_{\Gamma_t}, \mathbf{H}' >_{\Gamma_t}$ is the interface condition (ICS) for the TS model that will be presented in Section 2.4.

2.3. Coupling to global voltage for massive inductor

As presented in Section 2.2, the BC of $< \mathbf{n} \times \mathbf{E}, \mathbf{H}' >_{\Gamma_e - \Gamma_t}$ is the case for coupling to global quantity defined as a voltage V_i that is given in (4 a). Based on the development

in [4], the first problem defined in Ω_1 with a massive inductor alone is defined as

$$\partial_t(\mu\, \mathbf{H}_r, \mathbf{H}')_{\Omega_1} + (\sigma^{-1} \text{rot}\, \mathbf{H}_r, \text{rot}\, \mathbf{H}')_{\Omega_{1,c}} = V_i. \quad (11)$$

For a massive inductor, (11) can be also presented as

$$\partial_t\phi + RI_i = V_i, \quad (12)$$

where ϕ is the magnetic flux and R is the resistance.

2.4. Thin shell model and actual volume

The solution of (10) is now considered as a SS for the TS model linked to the trace of $< [\mathbf{n} \times \mathbf{E}]_{\Gamma_t}, \mathbf{H}' >_{\Gamma_t}$ in (9) is presented as [4]

$$< [\mathbf{n} \times \mathbf{E}]_{\Gamma_t}, \mathbf{H}' >_{\Gamma_t} = \mathbf{n} \times \mathbf{E}|_{\Gamma_t^+} - \mathbf{n} \times \mathbf{E}|_{\Gamma_t^-}$$
$$= \langle \frac{1}{2} \Big[\mu\beta\partial_t(2\mathbf{H}_{c,t} + \mathbf{H}_{d,t}) + \frac{1}{\sigma\beta}\mathbf{H}_{d,t} \Big], \mathbf{H}'_{c,t} + \mathbf{H}'_{d,t} \rangle_{\Gamma_t^+}$$
$$+ \langle \frac{1}{2} \Big[\mu\beta\partial_t(2\mathbf{H}_{c,t} + \mathbf{H}_{d,t}) - \frac{1}{\sigma\beta}\mathbf{H}_{d,t} \Big], \mathbf{H}'_{c,t} \rangle_{\Gamma_t^-} \quad (13)$$

By substituting (13) into (10), one has a full weak form of the TS problem with the **H**-conform formulation, i.e,

$$\partial_t(\mu\, \mathbf{H}_r, \mathbf{H}')_{\Omega} + (\sigma^{-1} \text{rot}\, \mathbf{H}_r, \text{rot}\, \mathbf{H}')_{\Omega_c} + (\mu\mathbf{H}_s, \mathbf{H}')_{\Omega_c^c} +$$
$$\langle \frac{1}{2} \Big[\mu\beta\partial_t(2\mathbf{H}_{c,t} + \mathbf{H}_{d,t}) + \frac{1}{\sigma\beta}\mathbf{H}_{d,t} \Big], \mathbf{H}'_{c,t} + \mathbf{H}'_{d,t} \rangle_{\Gamma_t^+}$$
$$+ \langle \frac{1}{2} \Big[\mu\beta\partial_t(2\mathbf{H}_{c,t} + \mathbf{H}_{d,t}) - \frac{1}{\sigma\beta}\mathbf{H}_{d,t} \Big], \mathbf{H}'_{c,t} \rangle_{\Gamma_t^-} = 0,$$
$$\forall\, \mathbf{H}' \in \mathbf{H} \in \mathbf{H}_h^0 (\text{rot}; \Omega), (14)$$

The TS solution obtained in (14) are finally improved by an actual volume (or volume correction) via the constrain of VSs ($\mathbf{B}_{s,actual}$ and $\mathbf{E}_{s,actual}$) given by [3]:

$$\mathbf{B}_{s,actual} = (\mu_{actual} - \mu_{ts})(\mathbf{H}_{massive} + \mathbf{H}_{ts}) \quad (15)$$

$$\mathbf{E}_{s,actual} = -(\mathbf{E}_{massive} + \mathbf{E}_{ts}) \quad (16)$$

where, μ_{actual}, μ_{ts} are the permeablities of the actual volume and TS model, respectivley. The fields $\mathbf{H}_{massive}, \mathbf{H}_{ts}, \mathbf{E}_{massive}, \mathbf{E}_{ts}$ are respectively the magnetic field intensity and electric field computed from the massive coil and TS model.

2.4. Computation of Joule power losses

The joule power loss (P_{loss}) can be computed with the below excpression:

$$P_{loss} = \frac{1}{2} \int_\Omega \frac{J^2}{\sigma} d\Omega, \quad (17)$$

where, the field J is defined in the plate. In order to calculate P_{loss}, it can be performed by post-processing via the gauss point intergration along the thickness of the thin plate. For that, (17) becomes as

$$P_{loss} = \frac{1}{2} \int_\Omega \frac{J^2}{\sigma} d\Omega \approx \frac{1}{\sigma} \sum_{i=1}^n (\frac{d}{2} w_{g,i} J)^2, \quad (18)$$

where, d is the thickness of the thin plate, n is the number gauss points along the thickness and $w_{g,i}$ is the corresponding weight factor.

3. EDDY CURRENT COMPUTATION IN A THIN SHIELD

An application here is a shielding plate of a distribution transformer with parameters with the rated power 560kV, 22/0,4kV. The model of the shielding plate is indicated in Figure 3 [1]. Massive inductors are three bus bars imposing by three balanced phase currents (phase A, phase B and phase C): $I_A = I_m \sin(\omega t)$, $I_B = I_m \sin(\omega t - 120^0)$ and $I_C = I_m \sin(\omega t + 120^0)$. The thickness of shielding plate is 6 mm. The distance between massive inductors (bus bars) is 114 mm. The shielding plate is made of two different regions, where the region 2 is the non-magnetic material and the region 1 is the magnetic material. The conductivity and permeability are given in each case of the test.
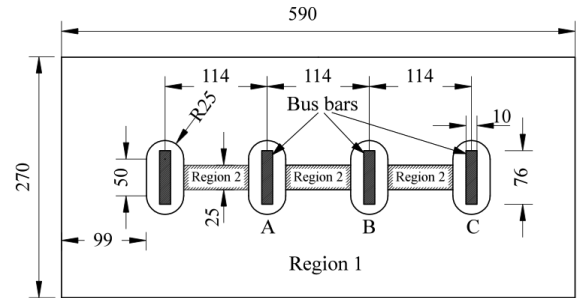
Fig. 3. Geometry of a shielding plate (dimensions are in mm) [1].

For the same material, one gets $\sigma_l = \sigma_{234} = 4.07 \times 10^6$ (S/m), $\mu_{r,1} = \mu_{r,234} = 300$ (relative magnetic permeabiltiy). The magnetic field distribution in a cut plane generated by global currents in the massive inductors is pointed out in Figure 5.
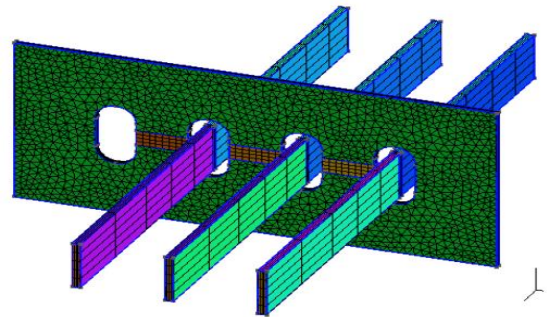
Fig. 4. A 3D mesh of the massive inductors and shielding plate.
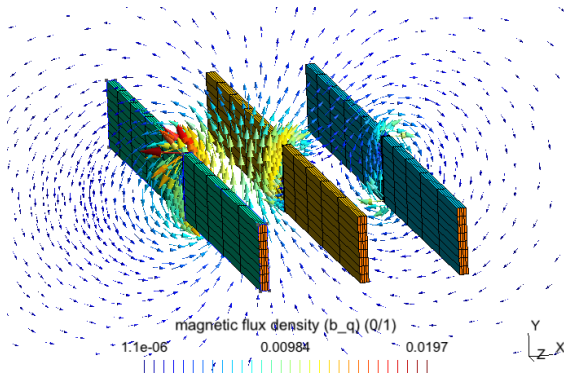
Fig. 5. Distribution of magnetic field in a cut plan.
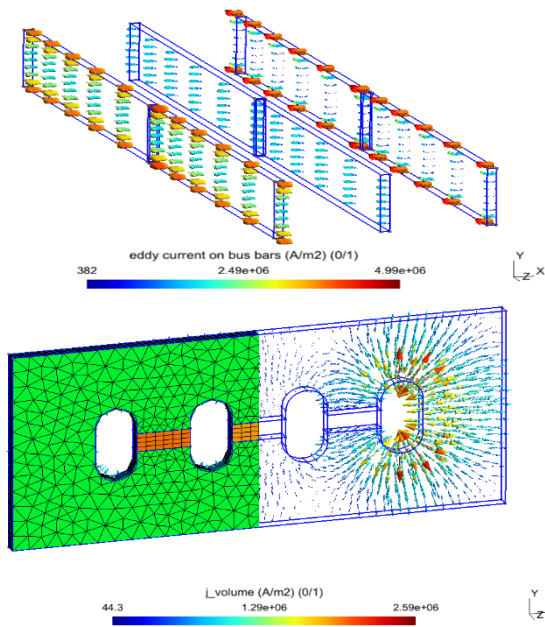
Fig. 6. Eddy current density in massive inductors (bus bars) (top) and a shielding plate (bottom).

For the same material, one gets $\sigma_1 = \sigma_{234} = 4.07 \times 10^6$ (S/m), $\mu_{r,1} = \mu_{r,2,3,4} = 300$. The magnetic field distribution in a cut plane due to the global currents is presented in Figure 5. The eddy current distributions in the massive inductors and shielding plate generated by the magnetic field distribution are shown in Figure 6. It is shown that the hightest current density appears in phase C (Fig 6, *bottom*). In addition, eddy current density is more intense near the conductor surface of massive inductors and the shielding plate (Fig 6, top) due to the skin effect. The comparison of distribution of eddy current densitythrough the hole and along the border of the shielding plate is shown in Figure 7. The obtained results are also performed by both models (TS model and actual volume). It is shown that the errors on the TS model is around 35% for both cases (f = 50Hz, skindepth $\delta = 2$ mm). In the similar way, for the case along the shielding plate, the discrepancy error between the TS and volume solutions is approximately 40% as in Figure 8. The

value of joule power loss density is 170W/m for the actual volume and 100W/m for the TS model.
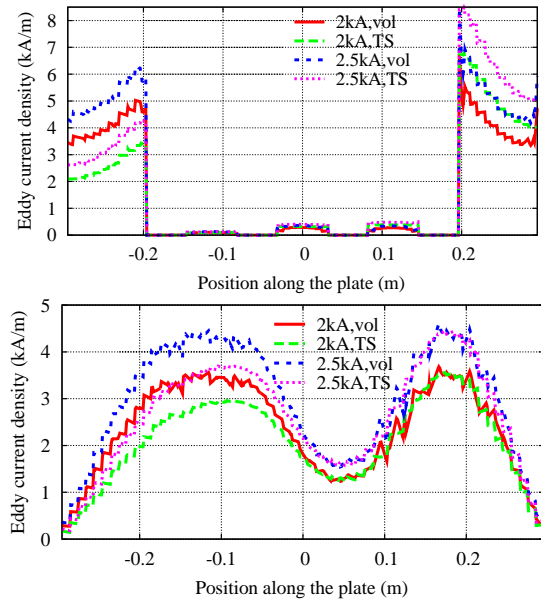
Fig. 7. Eddy current density distributions for the TS model and actual correction in the middle of the plate (*top*) and along the border of plate (*bottom*), with the same material.
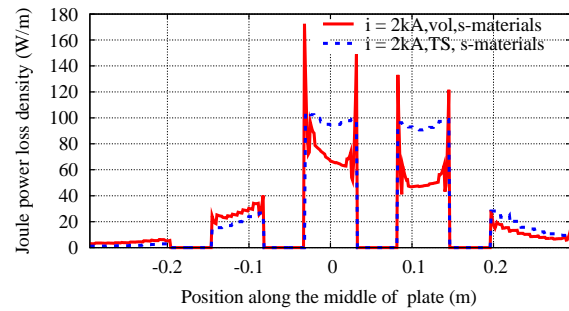
Fig. 8. Comparison of Joule power loss distributions through the hole of shielding plate with the same material.

Table 1. Comparison of Joule power loss density for each part with the same properties of the conductivity and relative pemeability ($\sigma_1 = \sigma_{234} = 4.07 \times 10^6$ (S/m); $\mu_{r,1} = \mu_{r,234} = 300$; $f = 50$Hz)

Same material	Joule power loss (W)	
	Thin Shell	FEM (vol)
Part-1	415,04	450,94
Part-2	5,337	5,782
Part-3	26,180	28,326
Part-4	25,115	27,146

It can be seen that the part 2 has the lowest joule power loss in comparison with the part 3 and part 4. This means

that this is the region with the smallest magnetic flux density.

For the different material, one gets: $\sigma_1 = 4.07 \times 10^6$ (S/m) $\sigma_{234} = 1.15 \times 10^6$ (S/m); $\mu_{r,1} = 300$; $\mu_{r,234} = 1$; $f = 50$Hz. It means that the part 1 is the magnetic material and part 2, 3 and 4 are the non magnetic materials. The joule power losse values of four parts with is given in Table 2.
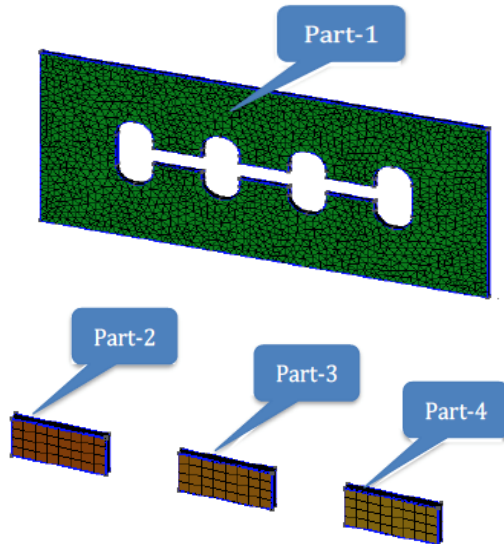
Fig. 9. A 3D mesh of the shielding plate with different parts (part 1, part 2, part 3 and part 4).

Table 2. The different properties of the conductivity and relative pemeability ($\sigma_1 = 4.07 \times 10^6$ (S/m); $\sigma_{234} = 1.15 \times 10^6$ (S/m); $\mu_1 = 300$; $\mu_{234} = 1$; $f = 50$Hz)

Different material	Joule power losses (W)	
	Thin Shell	Volume
Part-1	60,034	62.675
Part-2	0.002993	0.02767
Part-3	0.026545	0.01644
Part-4	0.03712	0.02347

4. CONCLUSION

The *h*-conform finite element perturbation approach has been successfully extended to field-circuit coupled problems. The extended formulations makes it possible to evaluate the local and global fields due to the electric current in the bus bars with affects of different properties. The results obtained from the proposed method have been shown a general picture of magnetic fields, eddy current and joule power losses in the bus bars and shielding plate with the same and different materials. Specially, the comparison of obtained results between the previous study for thin shell models (i.e., [3], [4]) and the proposed method was illustrated. This is also confirmed that there is a very good

agreement of the developed method in coupling to global quantities. In particular, this test example allows researchers and designers to evaluate the influence of the material properties on the shielding plate of the distribution transformer of 560kVA-22/0,4kV.

The source-code developed in this paper was based on the one proposed in [3], [4], [9]. This is the source-code developed by author and two professors (Patrick Dular and Christophe Geuzaine) at the University of Liege, Belgium. It will be then ran in the background of the Getdp and Gmsh that can be modified to be suitable with studied problems [12], [13].

In the future research, the coupling to global quantities could be expaned for multi shielding plates with the infuence of different materials (see e.g. [14]-[16]). Also, it could be extended for solving the practical problem in the time domain (see e.g. [17]).

REFERENCES

[1] K. Lakhiani; J. Turowski. Evaluation of Eddy Current Losses in the Cover Plates of Distribution Transformers. IET Proc. Sci. Meas. Technol. Vol. 151, No. 5, September 2004. http://dx.doi.org/10.1049/ip-smt:20040632

[2] P. Dular; R. V. Sabariego. A Perturbation Method for Computing Field Distortions Due to Conductive Regions With h -Conform Magnetodynamic Finite Element Formulations. In IEEE Transactions on Magnetics, vol. 43, no. 4, pp. 1293-1296, 2007. Doi: 10.1109/TMAG.2007. 892401.

[3] Vuong Q. Dang; P. Dular R.V. Sabariego; L. Krähenbühl; C. Geuzaine. Subproblem Approach for Modelding Multiply Connected Thin Regions with an h-Conformal Magnetodynamic Finite Element Formulation. In EPJ AP., vol. 63, no.1, 2013. https://doi.org/10.1051/epjap/ 2013120444.

[4] Vuong Q. Dang; P. Dular; R.V. Sabariego; L. Krähenbühl; C. Geuzaine. Subproblem approach for Thin Shell Dual Finite Element Formulations. IEEE Trans. Magn. Vol. 48, no. 2, pp. 407–410, 2012. Doi: 10.1109/TMAG.2011. 2176925.

[5] P. Dular, R. V. Sabariego, C. Geuzaine, M. V. Ferreira da Luz, P. Kuo-Peng, and L. Krahenbuhl, Finite element magnetic models via a coupling of subproblems of lower dimensions. In IEEE Transactions on Magnetics. Vol. 46, no. 8, pp. 2827-2830, 2010.

[6] K. Yamazaki; K. Muramatsu; M. Hirayama; A. Haga, and F. Torita. Optimal structure of magnetic and conductive layers of a magnetically shielded room. IEEE Trans. Magn. Vol. 42, no. 10, pp. 3524–3526, 2006. Doi: 10.1109/INTMAG. 2006.376530.

[7] M. D'Amore; E. Menghi; M. Sarto. Shielding techniques of the low-frequency magnetic field from cable power lines. Proc. IEEE Int. Symp. Electromagn. Compatibil. Vol. 1, pp. 203–208, 2003. Doi: 10.1109/ISEMC.2003.1236592

[8] T. Barbarics; A. Kost; D. Lederer; P. Kis. Electromagnetic field calculation for magnetic shielding with ferromagnetic material. IEEE Trans. Magn. Vol. 36, no. 4, pp. 986–989, 2000. Doi: 10.1109/20.877607

[9] Dang, V.Q. and Geuzaine, C. Two-way coupling of thin shell finite element magnetic models via an iterative subproblem method. COMPEL - The international journal for computation and mathematics in electrical and electronic engineering, Vol. 39 No. 5, pp. 1085-1097. https://doi.org/10.1108/ COMPEL-01-2020-0035.

[10] Vuong Dang Quoc. Modeling of Electromagnetic Systems by Coupling of Subproblems - Application to Thin Shell Finite Element Magnetic Models', PhD Thesis, 2013, University of Liege.

[11] S. Koruglu; P. Sergeant; R.V. Sabarieqo; Vuong. Q. Dang; M. De Wulf. Influence of contact resistance on shielding efficiency of shielding gutters for high-voltage cables. IET Electric Power Applications. Vol.5, No.9, pp. 715-720, 2011. Doi: 10.1049/iet-epa.2011.0081.

[12] GetDP, a general environment for the treatment of discrete problems, 1997-2012, http://www.geuz.org/getdp/.

[13] C. Geuzaine and J.-F. Remacle. Gmsh: a three-dimensional finite element mesh generator with built-in pre- and post-processing facilities. International Journal for Numerical Methods in Engineering 79(11), pp. 1309-1331, 2009.

[14] P. Thomas and Y. Le Menach, A three-dimensional electromagnetic shell finite element for coupled vector-scalar potential formulations, IEEE Transactions on Magnetics 48 (2012), no. 2, 823-826.

[15] M. Zucca, G. Lorusso, F. Fiorillo, P. E. Roccato, and M. Annibale, Highly efficient shielding of high-voltage underground power lines by pure iron screens, Journal of Magnetism and Magnetic Materials 320 (2008), 1065-1069.

[16] G. Eriksson, Efficient 3d simulation of thin conducting layers of arbitrary thickness, IEEE Transactions on Electromagnetic Compatibility (2007), 1-6.

[17] R. V. Sabariego, C. Geuzaine, P. Dular, and J. Gyselinck, Nonlinear timedomain finite element modeling of thin electromagnetic shells, IEEE Transactions on Magnetics 45 (2009), no. 3, 976-979.

[18] Vuong Dang Quoc Improvement of Shielding Models with h-Conformal Formulation using a Subproblem Finite Element Technique. GMSARN International Journal. Vol. 15, No. 02, pp. 121–126, 2021.

[19] Vuong Dang Quoc. Two-Way Procedure for Magnetostatic Finite Element Formulations via a Perturbation Method with Application to Thin Structures. GMSARN International Journal. Vol. 15, No. 03, pp. 231–235, 2021.